THE ROYAL SOCIETY

doi 10.1098/rspb.2000.1230

Gating energies and forces of the mammalian hair cell transducer channel and related hair bundle mechanics

Sietse M. van Netten[1*] **and Corné J. Kros**[2]

[1]*Department of Neurobiophysics, University of Groningen, Nijenborgh 4, 9747 AG Groningen, The Netherlands*
[2]*Department of Physiology, School of Medical Sciences, University of Bristol, University Walk, Bristol BS8 1TD, UK*

We quantified the molecular energies and forces involved in opening and closing of mechanoelectrical transducer channels in hair cells using a novel generally applicable method. It relies on a thermodynamic description of the free energy of an ion channel in terms of its open probability. The molecular gating force per channel as reflected in hair bundle mechanics is shown to equal $kT/I(X) \times \mathrm{d}I(X)/\mathrm{d}X$, where I is the transducer current and X the deflection of the hair bundle. We applied the method to previously measured $I(X)$ curves in mouse outer hair cells (OHCs) and vestibular hair cells (VHCs). Contrary to current models of transduction, gating of the transducer channel was found to involve only a finite range of free energy ($< 10\,kT$), a consequence of our observation that the channel has a finite minimum open probability of *ca.* 1% for inhibitory bundle deflections. The maximum gating forces per channel of both cell types were found to be comparable (*ca.* 300–500 fN). Because of differences in passive restoring forces, gating forces result in very limited mechanical nonlinearity in OHC bundles compared to that in VHC bundles. A kinetic model of channel activation is proposed that accounts for the observed transducer currents and gating forces. It also predicts adaptation-like effects and spontaneous bundle movements ensuing from changes in state energy gaps possibly related to interactions of the channel with calcium ions.

Keywords: electromechanical transduction; vestibular and outer hair cells; gating force; free energy; ion channels; hair bundle mechanics

1. INTRODUCTION

The opening and closing of mechanically gated ion channels in hair cells lies at the very core of our hearing ability. Determination of the related gating forces may take advantage of a unique feature of these mechanically gated channel proteins: a natural mechanical handle provided by the cell's characteristic organelle, the hair bundle. The hair bundle consists of a cluster of tens to hundreds of specialized microvilli called stereocilia. When deflected within a range of a few hundred nanometres, they modulate a channel's open probability from approximately zero to up to unity (Holton & Hudspeth 1986; Assad *et al.* 1989; Crawford *et al.* 1989; Géléoc *et al.* 1997). The channel protein's precise location in the cell membrane is still under debate (Denk *et al.* 1995; Hackney & Furness 1995; Lumpkin & Hudspeth 1995), although it has become clear that it must reside somewhere at the hair bundle's tip, each stereocilium most probably possessing one or possibly two channels. No molecular details of the channel are known (García-Añoveros & Corey 1997).

The exact machinery that transforms the deflection of a hair cell's sensory bundle into a force on the transducer channel's gate is still unknown. It is widely assumed that hair bundle deflection changes the tension in 'gating springs', elastic elements that pull directly on the ion channels' gates, thus changing the open probability of the channels. This model implies that hair bundle stiffness decreases if channels open, as first observed in hair cells of lower vertebrates (Howard & Hudspeth 1988). However, such clear signs of gating forces are not found in all types of hair cells. In studies on turtle and mouse auditory hair cells a causal relationship between hair bundle mechanics and gating of the transducer channel could not be demonstrated (Crawford *et al.* 1989; Russell *et al.* 1992; Géléoc *et al.* 1997).

Gating forces acting on the transducer channels in frog saccular hair cells have previously been determined by combining experimental data on nonlinear hair bundle dynamics with assumptions about the putative engaging elements, i.e. the gating springs (Howard & Hudspeth 1988). Here, we determine gating forces using a novel approach which is independent of any specific engagement model. Instead, it relies purely on fundamental thermodynamic properties of a gateable ion channel and the current being gated. When applied to transducer current measurements of mammalian hair cells of neonatal mice (Géléoc *et al.* 1997) it allows for quantification of the gating forces.

In order to account for the gating forces obtained we propose a new activation model of the transducer channel in which a linear elastic element differentially engages three kinetic states. The physical parameters of this model, namely the elastic constant of the activation element, the three different positions at which the hair bundle engages the three states and the two energy gaps between the three states, are obtained. A possible direct action of Ca^{2+} on the channel affecting the energy gaps between the states is discussed. In this scheme, Ca^{2+} may modulate the channel's open probability during Ca^{2+} inflow, giving rise to adaptation-like phenomena and resetting of the hair bundle's resting position.

*Author for correspondence (s.van.netten@phys.rug.nl).

2. MATERIAL AND METHODS

(a) *Experimental data*

Most of the experimental data on which the analysis in this work is based have been described in an earlier paper (Géléoc *et al.* 1997). Dr W. Marcotti contributed additional single-channel data from one outer hair cell (OHC). Transducer currents (I) were measured in OHCs and vestibular hair cells (VHCs) in organotypic cultures of neonatal mice. Cells were held at a potential of −84 mV and transducer currents were measured in whole-cell mode for 4 ms after the onset of a hydrodynamic velocity step stimulus in order to minimize interference of any transducer current adaptation. The hair bundle's tip displacement (X) was simultaneously measured using laser differential interferometry (Denk & Webb 1990). Step stimuli varying in amplitude allowed the construction of $I(X)$ curves. The mean current (figure 1*a*) was obtained as follows: individual measured $I(X)$ curves with variable deflection steps of on average *ca.* 10 nm were linearly interpolated in order to obtain discrete deflection steps of 5 nm and subsequently averaged. Our finding that a plateau of finite open probability exists (figure 1*b*) was based on measurements of single-channel activity in response to negative step deflection obtained from hair cells in which only one transducer channel was operational (Géléoc *et al.* 1997). A 50% threshold criterion for channel opening was applied to amplitude histograms (bin width 1 pA). Predicted false events due to baseline noise were corrected for by subtracting the number of samples > 5.0 pA from the total number of samples < -5.0 pA (the single-channel current was −10 pA at −84 mV). The absolute open probability at *ca.* −45 nm was estimated as 0.0087 ± 0.0018 (mean ± s.e.m.) ($n = 3$ OHCs).

(b) *Determination of $F_g(X)$ from $p_O(X)$ and $I(X)$*

An ion channel is assumed to be described by a multikinetic-state model in which the states with energies ε_i are indexed for the open (i_o) or closed (i_c) states. Then the channel's ensemble-averaged open probability under thermal equilibrium conditions (p_O) is dependent on the state energies ε_i according to the Boltzmann distribution:

$$p_O(x) = \frac{\sum_{i_o} \exp[-\varepsilon_i(x)/kT]}{\sum_{i_o, i_c} \exp[-\varepsilon_i(x)/kT]} = \sum_{i_o} \exp[-\varepsilon_i(x)/kT]/Q_{ch}(x), \quad (1)$$

where k is Boltzmann's constant and absolute temperature is indicated by T (e.g. Landau & Lifshitz 1980). The state energies are assumed to be dependent on x, the position of the engaging point of the transducer channel. The canonical partition function $Q_{ch}(x) = \exp(-A_{ch}(x)/kT)$ is introduced in order to relate the (Helmholtz) free energy of the channel $A_{ch}(x)$ to $p_O(x)$ yielding

$$A_{ch}(x) = A_g(x) + kT \ln\left[\sum_{i_o} \exp(-\varepsilon_i(x)/kT)\right], \quad (2)$$

where $A_g(x) = kT \ln p_O(x)$ equals the free energy difference between the equilibrium distribution over conformational states at x and the open configuration at x. We will assume only one open state with energy ε_O. Then the channel's free energy (A_{ch}) reduces to

$$A_{ch} = A_g + \varepsilon_O. \quad (3)$$

The derivative of the channel's free energy with respect to displacement of the engaging point of the channel, assuming constant temperature, equals the ensemble averaged force (f_{ch}) exerted on the channel:

$$f_{ch}(x) = \left.\frac{\partial A_{ch}}{\partial x}\right|_T = kT \frac{d[\ln(p_O(x))]}{dx} + \frac{d\varepsilon_O(x)}{dx}. \quad (4)$$

The first term on the right-hand side is associated with transitions between the closed and open states and is thus termed the gating force (f_g). The second term depends only on how displacement of the channel's engaging point modulates the potential energy of the channel's open state. If the position of the tip of the hair bundle (X) is related to that of the engaging point of the channel (x) via a lever ratio (γ) ($x = \gamma X$) (e.g. Howard *et al.* 1988), then the force on the channel as measured at the tip (F_{ch}) is

$$F_{ch}(X) = \gamma f_{ch} = F_g(X) + F_O(X), \quad (5)$$

with

$$F_O(X) = \frac{d\varepsilon_O(X)}{dX} \quad (6)$$

and

$$F_g(X) = kT \frac{d[\ln(p_O(X))]}{dX} = kT \frac{1}{I(X)} \frac{dI(X)}{dX}. \quad (7)$$

The last equals sign, which expresses the gating force per transducer channel as sensed at the tip of a hair bundle, implies statistical independence of all the transducer channels of a hair cell and assumes them to possess identical properties and modes of engagement so that their gated currents contribute equally to the transducer current (I) in response to hair bundle deflection (X).

The force required to deflect a hair bundle ($F_{hb}(X)$) with N_{ch} operational transducer channels is given by

$$F_{hb}(X) = S_p X + N_{ch} F_{ch}(X) - F_c, \quad (8)$$

where S_p accounts for the passive restoring stiffness related to the pivoting of the hair bundle in the cuticular plate (Crawford & Fettiplace 1985) and possible passive elastic contributions of side-to-side links connecting the stereocilia (Pickles *et al.* 1984; Hackney & Furness 1995; Furness *et al.* 1997) and F_c denotes a constant offset force for fulfilling $F_{hb}(0) = 0$.

(c) *Determination of total harmonic distortion*

The total harmonic distortion (THD) of hair bundle motion was determined from Fast Fourier Transforms of calculated displacement responses according to

$$\mathrm{THD} = 20 \times \log\left[\frac{\sum_{n=0, n\neq 1}^{15} |a_n|}{|a_1|}\right], \quad (9)$$

where a_0 is the amplitude of the DC component, a_1 is the amplitude of the principal component and a_n is the amplitude of the nth harmonic component.

3. RESULTS

(a) *Outer hair cells*

The steps for obtaining the gating force from experimentally determined curves of the transducer current

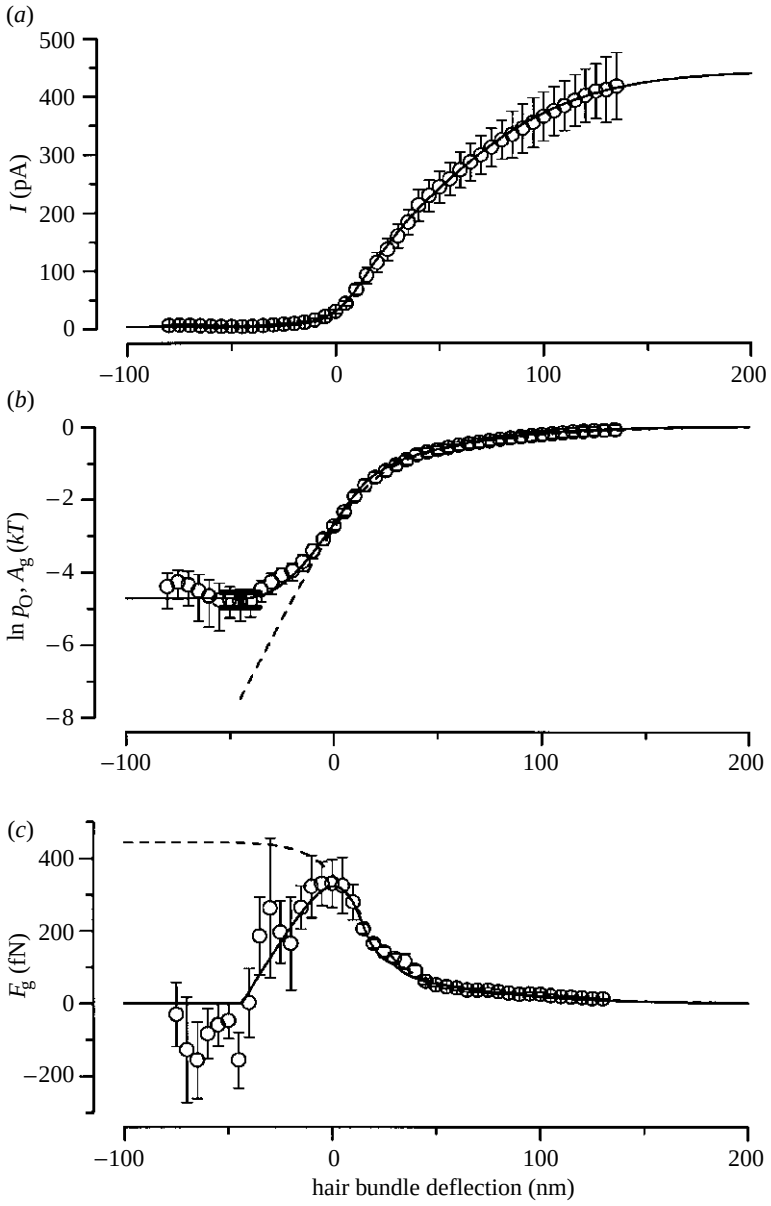

Figure 1. Mechanoelectrical transduction in cochlear OHCs. (*a*) Data points depict the (inward) OHC transducer current I (mean ± s.e.m., $n = 8$) measured as a function of deflection of the hair bundle 4 ms after the onset of a hydrodynamic velocity step applied to the bundle. The holding potential is −84 mV. The solid line shows the transducer current calculated according to $I = I_{max} p_O$ using equation (1) in combination with the energies of the three differentially activated states $\varepsilon_{C_1}(X)$, $\varepsilon_{C_2}(X)$ and $\varepsilon_O(X)$ as depicted in figure 2*a*. $I_{max} = 445$ pA. (*b*) Relationship between the logarithm of channel open probability or gating energy A_g (mean ± s.e.m., $n = 8$) and hair bundle deflection based on the data points in (*a*) normalized to $I_{max} = 445$ pA. The solid line represents the same model results as represented in (*a*). The dashed line shows the calculated open probability of a three-state (C_1, C_2 and O), continuously activating model (see Géléoc *et al*. 1997) ($a_1 = 0.085\ nm^{-1}$, $a_2 = 0.025\ nm^{-1}$, $x_1 = 17$ nm and $x_2 = 43$ nm). Clearly that model does not account for the non-zero open probability as observed at negative deflections (< −50 nm). The thick error bar indicates the range of channel open probabilities determined from single-channel activity at −45 nm. (*c*) Gating force F_g (mean ± s.e.m.) as a function of hair bundle deflection determined by applying equations (5)–(7) to the same eight individual current traces as used for figure 1*a* and subsequent averaging. The solid curve denotes the gating force following from the results of the differentially activating model also shown by the solid curves in figure 1*a*,*b*. The dashed line shows the gating force calculated with the continuously activating model, of which the open probability is depicted by the dashed line shown in figure 1*b*.

($I(X)$) of neonatal mouse OHCs are illustrated in figure 1. The transducer current in these cells typically starts to saturate at (positive) deflections towards the kinocilium exceeding a few hundred nanometres (figure 1*a*), but also approaches a small non-zero constant value at negative displacements. The behaviour at these negative displacements becomes clearer when the related open probability (p_O) of figure 1*a* is replotted on a logarithmic scale (figure 1*b*). The logarithm of open probability of a single ion channel equals the difference in free energy of gating (ΔG) per kT (equation (2)). Figure 1*b* thus shows that the full modulation of open probability of the transducer channel involves a finite range of free energy differences related to gating of *ca*. 5kT. This behaviour differs from current quantitative models of hair cell transduction (Corey & Hudspeth 1983; Holton & Hudspeth 1986; Howard & Hudspeth 1988; Crawford *et al*. 1989, 1991; Assad & Corey 1992; Shepherd & Corey 1994; Géléoc *et al*. 1997). Those models are based on differences in the channel's state energies that are linear with hair bundle deflection over their full range. They are thus all based on linear Boltzmann statistics, consistent with a continuously engaging linear gating spring, which puts no lower limit on the logarithm of the open probability of the channel's gate (dashed line in figure 1*b*). The finite open probability at inhibitory displacements also deviates from the deactivation of several voltage-gated channels, of which no such non-zero lower limit of open probability has been reported (Bezanilla & Stefani 1994). The ensemble averaged gating forces (figure 1*c*) in OHCs obtained using the thermodynamic approach (equations (5)–(7)) are found to be maximal (mean ± s.e.m. 330 ± 65 fN) ($n = 8$) close to the resting position of the hair bundle. At positive deflections, the gating forces gradually decline to zero. At the level of the micromechanics of a hair bundle's tip this decline is sensed as a reduction in its stiffness (dF_g/dX). This stiffness reduction reaches its minimal value ($-16 \pm 5\ \mu N\ m^{-1}$) per transducer channel at a deflection of *ca*. 10 nm, at which point the open probability is *ca*. 0.16. This reduction is completely analogous to but approximately a factor of three higher than the observed gating compliance per transducer channel (*ca*. $-5\ \mu N\ m^{-1}$) as

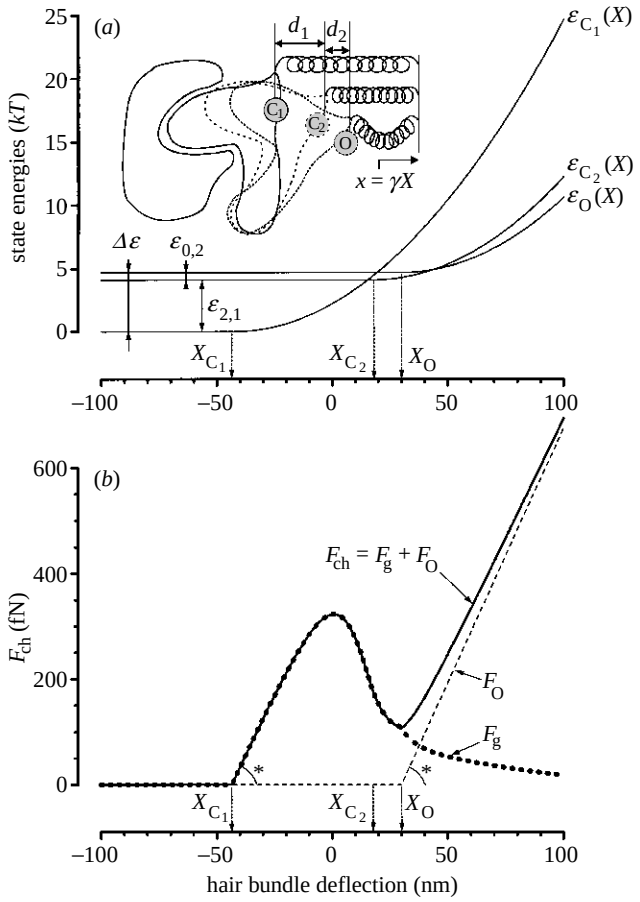

Figure 2. Differentially activating, three-state model for mechanoelectrical transduction. (*a*) Energies (ε_{C_1}, ε_{C_2} and ε_O) of the three states as a function of hair bundle deflection. Each state has its specific engaging position (X_{C_1}, X_{C_2} and X_O) beyond which it is activated by a linear elastic element. These positions are related via the geometrical constant γ to the discrete jumps (d_1 and d_2) that the gate makes between the different conformations, as depicted in the inset. Inset, schematic illustration of the three states of the transducer channel in a situation in which the hair bundle is deflected over a distance X with $X_{C_2} < X < X_O$. This corresponds to only the closed states (C_1 and C_2) being activated. The parameters are as used for the fits (solid lines) in figure 1 ($X_{C_1} = -43$ nm, $X_{C_2} = 18$ nm, $X_O = 30$ nm, $\varepsilon_{2,1} = 4.1\,kT$, $\varepsilon_{O,2} = 0.6\,kT$ and $K_{gs} = 9.6\,\mu N\,m^{-1}$). (*b*) Forces on the transducer channel (F_{ch}) obtained from the parameters illustrated in figure 2*a* and equations (5)–(7). F_g is the gating force and $F_O = d\varepsilon_O/dX$ represents the force exerted on the elastic element in the open state. Since the elastic element is assumed to be state independent, the slope of F_{ch} at $X_{C_1} = -43$ nm equals that of the asymptote for large positive deflections, as indicated by an asterisk.

inferred from observations on saccular hair cells (Howard & Hudspeth 1988). In response to negative hair bundle deflection the gating force also drops and, at *ca.* −50 nm, reaches values close to zero. From equations (5)–(7) it follows that a small or zero gating force at more negative displacements is directly related to the deflection-independent, non-zero open probability observed at these deflections (figure 1*b*). A zero gating force at deflections more negative than *ca.* −50 nm may be interpreted as a mechanical deactivation of the transducer channel's gate.

(b) *Differentially activating model of the transducer channel*

In order to account for mechanical disengagement of the transducer channel's gating machinery, we assumed that the channel possesses two closed states (C_1 and C_2) and one open state (O), of which the state energies (ε_{C_1}, ε_{C_2} and ε_O) are only partly and differentially dependent on hair bundle displacement (figure 2*a*). The present model is equivalent to a linear elastic element that is attached to the channel's gate at one side. The element's other side is assumed to be activated by the hair bundle, its displacement x being a geometrical factor γ of the hair bundle's tip deflection X ($x = \gamma X$) (inset in figure 2*a*). The elastic element is supposed to be string-like ('gating string') and, thus, cannot exert pushing (negative) forces on the gate. When in conformational state C_1, the element only tensions the gate if the hair bundle deflection X is more positive than a fixed engaging position X_{C_1} (figure 2*a*). If it is assumed that the channel's gate is displaced over a discrete distance d_1 when the channel switches from state C_1 to C_2, the elastic element will only activate the gate in the C_2 state if the hair bundle is deflected beyond the engaging position $X_{C_2} = X_{C_1} + d_1/\gamma$. Similarly, the open state's energy is only affected by the elastic element if the hair bundle is deflected beyond position $X_O = X_{C_2} + d_2/\gamma$, where d_2 is the gate's discrete swing between the C_2 and O states. The elastic element's linear stiffness (k_{gs}) is assumed to be state independent. It will thus raise the energies of all three states by the same proportion as the square of hair bundle deflection beyond their respective engaging positions (figure 2*a*), contrary to a previously proposed three-state scheme with a slackening gating spring (Markin & Hudspeth 1995). Our model also deviates crucially from the mathematical description of the gating spring model in which the state energies are mirror symmetrical with respect to the present engaging positions (Howard & Hudspeth 1988; Corey & Howard 1994; Markin & Hudspeth 1995). The distribution over the three states and the related open probability and gating forces of this differentially activating model were determined using equations (1) and (5)–(7). The three engaging positions (X_{C_1}, X_{C_2} and X_O) beyond which the three states are tensioned, the two disengaged energy gaps between the three states ($\varepsilon_{2,1} = \varepsilon_{C_2} - \varepsilon_{C_1}$ and $\varepsilon_{O,2} = \varepsilon_O - \varepsilon_{C_2}$) and the elastic element's stiffness as sensed at the tip of the hair bundle $K_{gs}(=\gamma^2 k_{gs})$ were adjusted to fit the model to the measured data (solid lines in figure 1). These six physical parameters fully determine the total force on a transducer channel (F_{ch}) which equals the gating force (F_g) plus the force (F_O) needed to extend the elastic element if the channel is in its open state (equations (5)–(7)). In the present model, evaluation of $F_O = d\varepsilon_O/dX$ yields $F_O = 0$ if $X < X_O$ and $F_O = K_{gs}(X - X_O)$ if $X \geqslant X_O$. Both F_g and F_O plus the total force as obtained from the fitted parameters are shown in figure 2*b*.

(c) *Vestibular hair cells*

In order to investigate whether the present differentially activating model of hair cell transduction is more generally usable we applied it to another mammalian hair cell preparation: cultured mouse VHCs. In contrast to those of OHCs, measurements of the forces required to

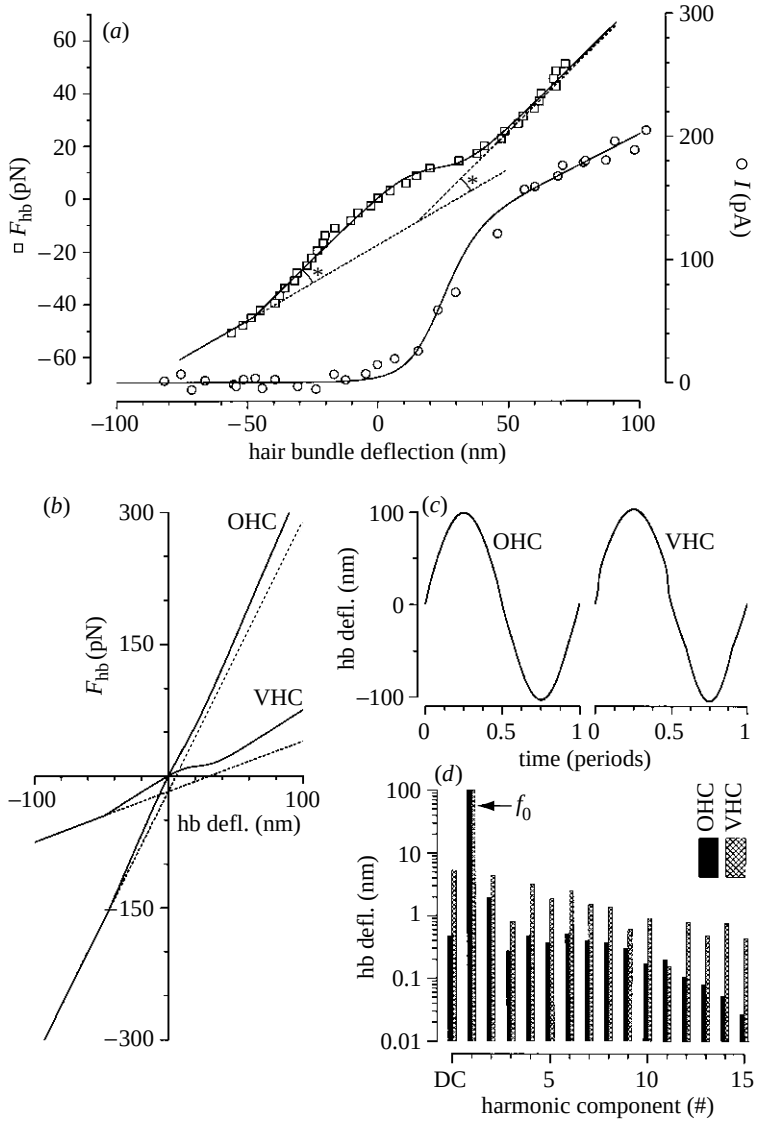

Figure 3. Application of the differentially activating, three-state model to experimental results of VHCs and comparison to OHCs. (*a*) Experimentally determined forces on a hair bundle (squares) and evoked transducer currents (circles) of a VHC as a function of deflection (Géléoc *et al.* 1997). The forces obtained from displacement measurements were scaled by a factor of 0.55. Solid lines represent fits of the differentially activating, three-state model. Lower dashed line represents the forces related to the passive stiffness (S_p) of the stereocilia. The upper dashed line is $S_{p,VHC} \times X + N_{ch,VHC} \times F_O(X)$. Asterisks indicate identical slopes (see § 3). The parameters are $X_{C_1} = -47$ nm, $X_{C_2} = 10$ nm, $X_O = 15$ nm, $\varepsilon_{2,1} = 6.2\,kT$, $\varepsilon_{O,2} = 0.94\,kT$, $K_{gs} = 9.7\,\mu N\,m^{-1}$, $S_{p,VHC} = 572\,\mu N\,m^{-1}$ and $N_{ch,VHC} = 42$. (*b*) Comparison of force deflection relationships of VHC and OHC bundles (solid lines) as derived from fits (figures 1 and 3*a*) ($S_{p,OHC} = 3.05\,mN\,m^{-1}$ and $N_{ch,OHC} = 48$) of the differentially activating model. Deviation of F_{hb} from the linear behaviour of the passive stiffness forces (dashed curves) is due to gating mechanics and is similar in magnitude for both cell types. (*c*) Calculations of hair bundle displacements in response to sinusoidal fluid flow past the hair bundles (e.g. Van Netten 1997) based on the $F_{hb}(X)$ curves depicted in (*b*). The differences in the relative contribution of forces related to the channel gating and those resulting from the passive stereociliary stiffness result in markedly different distortion for the two types of hair cells. (*d*) Harmonic components of distorted hair bundle responses obtained by taking a Fast Fourier Transform of the two waveforms shown in (*c*). The fundamental component indicated by f_0 is the response at the stimulus frequency.

deflect the hair bundle ($F_{hb}(X)$) revealed clear nonlinear mechanical behaviour presumably related to gating of the transducer channels (Géléoc *et al.* 1997). If the differentially activating model were to be correct we would expect the sum of the thermodynamically determined gating forces ($N_{ch}F_g$, where N_{ch} is the number of operational channels) to equal the nonlinearities in the measured forces on the hair bundles, i.e. $F_{hb}(X)$. Figure 3*a* shows the measured transducer current (circles) of a VHC together with the fitted model (solid line). Assuming a single-channel transducer conductance of 112 pS (Géléoc *et al.* 1997) and fitting the model to the measured currents, we arrived at an estimate of 42 operational transducer channels in this cell. The six physical parameters resulting from the fit were used to calculate the total force needed in order to gate these 42 transducer channels. This force was added to a linearly increasing force (lower dashed line in figure 3*a*), which is commonly associated with the passive restoring stiffness (S_p) of stereocilia (equation (8)). Clearly, the measured forces, i.e. $F_{hb}(X)$ (squares),

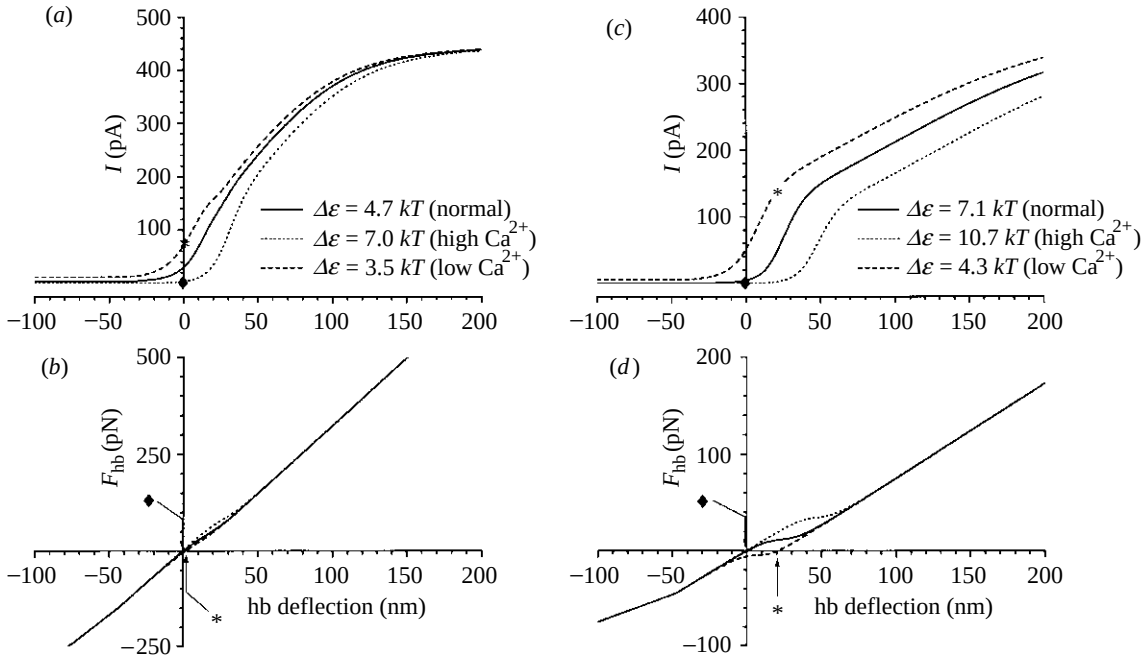

Figure 4. Calculated dependence of $I(X)$ and $F_{hb}(X)$ of OHCs and VHCs on the energy gap between the C_1 and O states, i.e. $\Delta\varepsilon$. The values of $\varepsilon_{O,2}$ and $\varepsilon_{2,1}$ are changed in proportion to $\Delta\varepsilon$. All other parameters were held fixed and equalled those given in the legends of figures 2 (OHCs) and 3 (VHCs). (*a*) Transducer current versus displacement of OHCs. The solid line represents the control situation shown in figure 1*a*, i.e. $\varepsilon_{2,1} = 4.12\,kT$ and $\varepsilon_{O,2} = 0.57\,kT$ ($\Delta\varepsilon = 4.7\,kT$), the dashed line simulates transduction under high Ca^{2+} concentration, i.e. $\varepsilon_{2,1} = 6.18\,kT$ and $\varepsilon_{O,2} = 0.86kT$ ($\Delta\varepsilon = 7.0kT$) and the short dashed line simulates transduction under low Ca^{2+} concentration, i.e. $\varepsilon_{2,1} = 3.1kT$ and $\varepsilon_{O,2} = 0.43\,kT$ ($\Delta\varepsilon = 3.5kT$). The diamond and asterisk indicate new resting positions (see (*b*)). (*b*) Force on hair bundle versus resulting deflection of OHCs calculated with the same parameters and indicated with similar lines as used in (*a*). The new resting positions (X_{rest}) of the hair bundle are diamond $X_{rest} \cong -0.1$ nm ($\Delta\varepsilon = 7.0kT$) and asterisk $X_{rest} \cong 1.5$ nm ($\Delta\varepsilon = 3.5kT$). (*c*) Transducer current versus displacement of VHC. The solid line represents the control situation shown in figure 3*a*, i.e. $\varepsilon_{2,1} = 6.20kT$ and $\varepsilon_{O,2} = 0.94kT$ ($\Delta\varepsilon = 7.1kT$), the dashed line simulates transduction under high Ca^{2+} concentration, i.e. $\varepsilon_{2,1} = 9.30kT$ and $\varepsilon_{O,2} = 1.41kT$ ($\Delta\varepsilon = 10.7kT$) and the short dashed line simulates transduction under low Ca^{2+} concentration, i.e. $\varepsilon_{2,1} = 3.72kT$ and $\varepsilon_{O,2} = 0.56kT$ ($\Delta\varepsilon = 4.3kT$). The diamond and asterisk indicate new resting positions (see (*d*)). (*d*) Force on hair bundle versus resulting deflection of VHC calculated with the same parameters and indicated with similar lines as used in (*c*). The new resting positions of the hair bundle are diamond $X_{rest} \cong -0.5$ nm ($\Delta\varepsilon = 10.7kT$) and asterisk $X_{rest} \cong 20.5$ nm ($\Delta\varepsilon = 4.3kT$).

accurately reflect the gating forces, i.e. $\mathcal{N}_{ch}F_g$ (deviation of the solid line from the two dashed lines), as calculated purely from the $I(X)$ curve. The similarity of the slope of the measured $F_{hb}(X)$ curve at the engaging position X_{C_1} (-47 nm) with that of the asymptote for large X (higher dashed line in figure 3*a*) supports the model assumption that the elastic element's stiffness is similar while engaging the C_1 or O conformational states.

(d) *Comparison of outer and vestibular hair cells and related mechanical distortion*

The ratio of the forces acting on the transducer channel to those resulting from the passive stiffness (S_p) determines to what extent opening and closing of the transducer channels affects the overall dynamics of a hair bundle. The magnitude of the forces acting on the transducer channels is strikingly similar for OHCs and VHCs. This is evident in figure 3*b* from the similarity of the differences between the forces required to deflect the bundle, i.e. F_{hb} (solid lines) and the forces associated with the linear passive stiffness, i.e. S_p (dashed lines). The passive stiffness of OHC bundles was found to be more than five times that of VHC bundles ($S_{p,OHC} \approx 3.05$ mN m^{-1} and $S_{p,VHC} \approx 0.57$ mN m^{-1}) (e.g. Géléoc *et al.* 1997). Accordingly, the force curve $F_{hb}(X)$, as obtained for OHCs (equation (8)), is markedly more linear than that for VHCs (figure 3*b*). Associated with this is the relatively low mechanical distortion of OHC bundle displacements caused by gating when forces resulting from a sinusoidally varying fluid flow past the hair bundles are applied. Figure 3*c* shows such calculated distorted hair bundle displacements (e.g. Van Netten 1997) of OHCs (THD $= -25.1$ dB) and VHCs (THD $= -12.3$ dB) at an amplitude of *ca.* 100 nm for both. The two force-deflection profiles ($F_{hb}(X)$) of figure 3*b* were used for these calculations and it was assumed that the bundles were driven at acoustic frequencies (f_0) at which viscous fluid forces dominate but adaptation (Eatock *et al.* 1987) is negligible. The spectral distributions of the responses in figure 3*c* are depicted in figure 3*d* for the first 15 harmonics and reveal significantly smaller distortion of OHC bundles in comparison to VHC bundles. The lowest even components dominate the distortion in the two spectra, particular those at DC and $2f_0$.

4. DISCUSSION

(a) *Relationship between molecular gating forces and gated current*

With the present thermodynamic approach, we have been able to relate molecular gating forces to the transducer currents being gated. Application to two types of mammalian hair cells yielded comparable gating forces, which were shown to result in different mechanical nonlinear behaviour of their bundles because of the differences in the passive restoring forces of the hair bundles. With respect to mechanical distortion of their hair bundles, mammalian VHCs thus bear more similarity to the nonlinear behaviour observed in frog saccular hair cells (Howard & Hudspeth 1988) and fish lateral line hair cells (Van Netten & Khanna 1994) than they do to OHCs.

The gating forces affect the OHC bundle in such a way that, at small deflections (<40 nm) around the equilibrium position, the hair bundle is less stiff in the excitatory than in the inhibitory direction (figure 3*b*). However, if the deflections around the equilibrium position become larger (>100 nm), the hair bundle appears to be effectively stiffer in the excitatory than in the inhibitory direction (e.g. Flock & Strelioff 1984).

The data for both hair cell types can be explained if the transducer channel is deactivated at deflections more negative than *ca.* -50 nm. We interpreted this as a mechanical disengagement, which has previously also been suggested to cause the discontinuities observed in saccular hair bundle mechanics and related kinetics at displacements more negative than *ca.* -100 nm (Corey & Hudspeth 1983; Howard & Hudspeth 1988; Shepherd & Corey 1994; Markin & Hudspeth 1995).

We found that, at deflections positive to *ca.* -50 nm, the force on the transducer channel (F_{ch}) first increases linearly with deflection, the slope reflecting the stiffness of the elastic element pulling on the channel's gate which is predominantly in the C_1 state (figure 2*b*). Deviation from this linear increase results from transitions from the C_1 state to the increasingly more favoured C_2 and O states and becomes significant when the bundle is close to the undeflected equilibrium position, at which the force on the channel is locally maximal (330 fN). This force can thus be interpreted as a measure of the bond strength of the C_1 state. Current hypotheses regarding site and activation of the transducer channel (Pickles *et al.* 1984; Howard & Hudspeth 1988; Howard *et al.* 1988; Pickles 1993; Hackney & Furness 1995; Furness *et al.* 1997) imply a geometrical factor γ in the ranges of *ca.* 0.05–0.07 (OHCs) and 0.02–0.04 (VHCs) based on the height of their stereocilia (OHCs 4–5 μm and VHCs 9–10 μm) and their similar rootlet spacing ($\approx$250 nm) (Géléoc *et al.* 1997). At the molecular level, this would imply a bond strength of the C_1 state of *ca.* 5.5 pN (330/γ fN) for OHCs and 15 pN (455/γ fN) for VHCs. Forces of this order of magnitude (10 pN) move the transmembrane voltage sensors that gate Na^+ channels, as can be inferred from a model for the transition from the closed to the open state of a single S4 sensor (French *et al.* 1996). Similar-sized forces have been found experimentally for unbinding motor molecules (Nishizaka *et al.* 1995) and they also represent a lower bound of observed receptor–ligand bonds (Merkel *et al.* 1999). Clearly, the open configuration is much more stable than the C_1 or C_2 configurations, since it may withstand forces of at least 20 pN which can be calculated to result from an OHC bundle deflection of 150 nm, which would result in a 95% saturated transducer current (Géléoc *et al.* 1997). Similarly, for VHCs a bond strenght of *ca.* 100 pN is obtained for the O state. Comparable maximal forces per transducer channel have been estimated on the basis of displacement clamp measurements on saccular hair cell bundles (Jaramillo & Hudspeth 1993).

(b) *Dependence of $I(X)$ and $F_{hb}(X)$ on the state energy gap and possible relationship to Ca^{2+} and adaptation*

Our model of transduction shows (figure 2*a*) that the energy gap ($\Delta\varepsilon$) between the deactivated lowest state (C_1) and deactivated highest state (O) of the OHC transducer channel is *ca.* $5kT$. This energy difference is directly related to the finite deactivated open probability ($p_{O,deact}$) at deflections more negative than *ca.* -50 nm, since it follows from equation (1) that

$$p_{O,deact} = p_O(X)|_{X<-50\,nm} \cong \exp[-(\varepsilon_O(X)-\varepsilon_{C_1}(X))/kT]|_{X<-50\,nm} \quad (10)$$

and, thus,

$$\Delta\varepsilon = \varepsilon_{2,1} + \varepsilon_{O,2} = [\varepsilon_O(X) - \varepsilon_{C_1}(X)]|_{X<-50\,nm} \cong -kT\ln p_{O,deact} \quad (11)$$

Obviously, values of the energy gap close to the thermal noise limit will cause a large proportion of channels to open spontaneously, effectively rendering them useless for signalling mechanical events and, thus, diminishing the instantaneous operational range. Figure 4*a*,*c* shows calculated transducer currents and figure 4*b*,*d* related hair bundle mechanics for both OHCs and VHCs at values for the energy gap $\Delta\varepsilon$ differing by a few kT while keeping all other parameters of the model fixed. An increased $\Delta\varepsilon$ shifts the $I(X)$ curves in the excitatory (positive) direction in both VHCs and OHCs and also makes them steeper in OHCs, while a decrease in $\Delta\varepsilon$ has the opposite effects. Similar shifts and/or slope changes of $I(X)$ curves have been observed experimentally in hair cells by varying extracellular Ca^{2+} or by changes in holding potential that presumably act by changing the driving force for Ca^{2+} entry through the transducer channels (Assad *et al.* 1989; Crawford *et al.* 1989, 1991; Kros *et al.* 1993). Whether the $I(X)$ curve simply shifted in our model or was accompanied by a slope change as well depended critically on the contribution of $\varepsilon_{2,1}$ and $\varepsilon_{O,2}$ to the change in $\Delta\varepsilon$. The larger the contribution of ε_O the more the $I(X)$ curves tended to shift solely (e.g. VHCs) (figure 4). This may be a partial explanation for a similar variation in experimental findings (Assad & Corey 1992). It has been proposed that these effects could effectively constitute transducer current adaptation and it was shown that the changes in $I(X)$ curves could be simulated by a change of a set point of transitions between the two closed states in a model based on linear second-order Boltzmann statistics (Crawford *et al.* 1989, 1991). Whatever the precise action of Ca^{2+} on the transducer channel

is, the change in the $I(X)$ curve concurrently affects hair bundle mechanics according to the combination of equations (5)–(8) (figure 4*b*,*d*). The undisturbed hair bundle assumes a new resting position (X_{rest}) which is defined by $F_{hb}(X_{rest}) = 0$. The value of X_{rest} becomes negative (diamond) as $\Delta\varepsilon$ increases and positive (asterisk) as $\Delta\varepsilon$ decreases. These shifts enhance the changes in the silent current $I(X_{rest})$. The effect is most apparent in VHCs for decreasing $\Delta\varepsilon$ (asterisk in figure 4*c*). These mechanical shifts are opposite to the effects of Ca^{2+} on hair bundles as observed in frog saccular hair cells, which were explained by assuming the control of a molecular motor (Assad *et al*. 1989). However, our shifts, which were predicted from a possible direct interaction of the channel with Ca^{2+}, agree with some recent observations on turtle hair bundles (Ricci *et al*. 2000). The discrepancy is consistent with the coexistence of two distinct adaptation mechanisms in the hair bundle (Wu *et al*. 1999) which may or may not be observed depending on the experimental conditions. In terms of the present model, hair bundle shifts resulting from a direct action of Ca^{2+} on the transducer channel's energy gaps are described by changes in F_{ch}, while the mechanical effects of a possible Ca^{2+}-dependent motor that modulates the tension in the elastic elements activating the channel can possibly be described by changes in its argument, i.e. X (equation (8)).

Figure 4 again illustrates that it is the ratio of the forces acting on the transducer channels to those related to the passive stiffness that affects hair bundle mechanics. In OHC bundles with a relatively large passive stiffness, the bundle mechanics hardly change, but in VHCs a clear effect is seen if $\Delta\varepsilon$ is changed. Thus, transducer-induced mechanical effects in the processing of signals by various hair cell types may differ significantly, whereas the underlying gating mechanics are similar.

Funding was provided via an EC Human Capital and Mobility Grant. We thank Dr N. P. Cooper, Dr J. H. van Hateren, Dr M. C. Holley, Dr A. B. A. Kroese and Professor D. G. Stavenga for commenting on previous versions of the manuscript and Dr W. Marcotti for contributing some of the experimental data.

REFERENCES

Assad, J. A. & Corey, D. P. 1992 An active motor model for adaptation by vertebrate hair cells. *J. Neurosci.* **12**, 3291–3309.

Assad, J. A., Hacohen, N. & Corey, D. P. 1989 Voltage dependence of adaptation and active bundle movement in bullfrog saccular hair cells. *Proc. Natl Acad. Sci. USA* **86**, 2918–2922.

Bezanilla, F. & Stefani, E. 1994 Voltage-dependent gating of ionic channels. *A. Rev. Biophys. Biomol. Struct.* **23**, 819–846.

Corey, D. P. & Howard, J. 1994 Models for ion channel gating with compliant states. *Biophys. J.* **66**, 1254–1257.

Corey, D. P. & Hudspeth, A. J. 1983 Kinetics of the receptor current in bullfrog saccular hair cells. *J. Neurosci.* **3**, 962–976.

Crawford, A. C. & Fettiplace, R. 1985 The mechanical properties of ciliary bundles of turtle cochlear hair cells. *J. Physiol.* **364**, 359–379.

Crawford, A. C., Evans, M. G. & Fettiplace, R. 1989 Activation and adaptation of transducer currents in turtle hair cells. *J. Physiol.* **419**, 405–434.

Crawford, A. C., Evans, M. G. & Fettiplace, R. 1991 The action of calcium on the mechano-electrical transducer current of turtle hair cells. *J. Physiol.* **434**, 369–398.

Denk, W. & Webb, W. W. 1990 Optical measurements of picometer displacements of transparent microscopic objects. *Appl. Opt.* **29**, 2382–2391.

Denk, W., Holt, J. R., Shepherd, G. M. G. & Corey, D. P. 1995 Calcium imaging of single stereocilia in hair cells: localization of transduction channels at both ends of tip links. *Neuron* **15**, 1311–1321.

Eatock, R. A., Corey, D. P. & Hudspeth, A. J. 1987 Adaptation of mechanoelectrical transduction in hair cells of the bullfrog's sacculus. *J. Neurosci.* **7**, 2821–2836.

Flock, A. & Strelioff, D. 1984 Graded and nonlinear mechanical properties of sensory hairs in the mammalian hearing organ. *Nature* **310**, 597–599.

French, R. J., Prusak-Sochaczewski, E., Zamponi, G. W., Becker, S., Shavantha Kularatna, A. & Horn, R. 1996 Interactions between a pore-blocking peptide and the voltage sensor of the sodium channel: an electrostatic approach to channel geometry. *Neuron* **16**, 407–413.

Furness, D. N., Zetes, D. E., Hackney, C. M. & Steele, C. R. 1997 Kinematic analysis of shear displacement as a means for operating mechanotransduction channels in the contact region between adjacent stereocilia of mammalian cochlear hair cells. *Proc. R. Soc. Lond.* B **264**, 45–51.

García-Añoveros, J. & Corey, D. P. 1997 The molecules of mechanosensation. *A. Rev. Neurosci.* **20**, 567–594.

Géléoc, G. S. G., Lennan, G. W. T., Richardson, G. P. & Kros, C. J. 1997 A quantitative comparison of mechanoelectrical transduction in vestibular and auditory hair cells of neonatal mice. *Proc. R. Soc. Lond.* B **264**, 611–621.

Hackney, C. M. & Furness, D. N. 1995 Mechanotransduction in vertebrate hair cells: structure and function of the stereociliary bundle. *Am. J. Physiol.* **268**, C1–C13.

Holton, T. & Hudspeth, A. J. 1986 The transduction channel of hair cells from the bull-frog characterized by noise analysis. *J. Physiol.* **375**, 195–227.

Howard, J. & Hudspeth, A. J. 1988 Compliance of the hair bundle associated with gating of mechanoelectrical transduction channels in the bullfrog's saccular hair cell. *Neuron* **1**, 189–199.

Howard, J., Roberts, W. M. & Hudspeth, A. J. 1988 Mechanoelectrical transduction by hair cells. *A. Rev. Biophys. Biophys. Chem.* **17**, 99–124.

Jaramillo, F. & Hudspeth, A. J. 1993 Displacement-clamp measurement of the forces exerted by gating springs in the hair bundle. *Proc. Natl Acad. Sci. USA* **90**, 1330–1334.

Kros, C. J., Rüsch, A., Lennan, G. W. T. & Richardson, G. P. 1993 Voltage dependence of transducer currents in outer hair cells of neonatal mice. In *Biophysics of hair cell sensory systems* (ed. H. Duifhuis, J. W. Horst, P. Van Dijk & S. M. van Netten), pp. 141–150. Singapore: World Scientific.

Landau, L. D. & Lifshitz, E. M. 1980 *Statistical physics*, vol. 1, 3rd edn. Oxford, UK: Pergamon Press.

Lumpkin, E. A. & Hudspeth, A. J. 1995 Detection of Ca^{2+} entry through mechanosensitive channels localizes the site of mechanoelectrical transduction in hair cells. *Proc. Natl Acad. Sci. USA* **92**, 10 297–10 301.

Markin, V. S. & Hudspeth, A. J. 1995 Gating-spring models of mechanoelectrical transduction by hair cells of the internal ear. *A. Rev. Biophys. Biomol. Struct.* **24**, 59–83.

Merkel, R., Nassoy, P., Leung, A., Ritchie, K. & Evans, E. 1999 Energy landscapes of receptor–ligand bonds explored with dynamic force spectroscopy. *Nature* **397**, 50–53.

Nishizaka, T., Miyata, H., Yoshikawa, H., Ishiwata, S. & Kinosita, K. 1995 Unbinding force of a single motor molecule of muscle measured using optical tweezers. *Nature* **377**, 251–254.

Pickles, J. O. 1993 A model for the mechanics of the stereociliar bundle on acousticolateral hair cells. *Hearing Res.* **68**, 159–172.

Pickles, J. O., Comis, S. D. & Osborne, M. P. 1984 Cross-links between stereocilia in the guinea pig organ of Corti, and their possible relation to sensory transduction. *Hearing Res.* **15**, 103–112.

Ricci, A. J., Fettiplace, R. & Crawford, A. C. 2000 Active hair bundle movements during hair cell depolarization. *Assoc. Res. Otolaryngol. Abs.* **23**, 768.

Russell, I. J., Kössl, M. & Richardson, G. P. 1992 Nonlinear mechanical responses of mouse cochlear hair bundles. *Proc. R. Soc. Lond.* B **250**, 217–227.

Shepherd, G. M. G. & Corey, D. P. 1994 The extent of adaptation in bullfrog saccular hair cells. *J. Neurosci.* **14**, 6217–6229.

Van Netten, S. M. 1997 Harmonic distortion of cupular mechanics generated by the gating springs of lateral line hair cells. In *Diversity in auditory mechanics* (ed. E. R. Lewis, G. R. Long, R. F. Lyon, P. M. Narris, C. R. Steele & E. Hecht-Poinar), pp. 594–600. Singapore: World Scientific.

Van Netten, S. M. & Khanna, S. M. 1994 Stiffness changes of the cupula associated with the mechanics of hair cells in the fish lateral line. *Proc. Natl Acad. Sci. USA* **91**, 1549–1553.

Wu, Y.-C., Ricci, A. J. & Fettiplace, R. 1999 Two components of transducer adaptation in auditory hair cells. *J. Neurophysiol.* **82**, 2171–2181.

As this paper exceeds the maximum length normally permitted, the authors have agreed to contribute to production costs.